Fibrillar Chromospheric Spicule-Like Counterparts to an EUV and Soft X-Ray Blowout Coronal Jet

Alphonse C. Sterling[1]

Space Science Office, VP62, NASA Marshall Space Flight Center, Huntsville, AL 35812

USA

alphonse.sterling@nasa.gov

Louise K. Harra

Mullard Space Science Laboratory, University College London, Holmbury St. Mary,

Dorking, Surrey, RH5 6NT, UK

and

Ronald L. Moore

NASA/Marshall Space Flight Center, VP62/Space Science Office, Huntsville, AL 35805

USA

ron.moore@nasa.gov

Received ⸻; accepted ⸻

[1]Current address: JAXA/Institute of Space and Astronautical Science, Hinode Group, 3-1-1 Yoshinodai, Sagamihara, Kanagawa 229-8510, Japan

ABSTRACT

We observe an erupting jet feature in a solar polar coronal hole, using data from *Hinode*/SOT, EIS, and XRT, with supplemental data from *STEREO*/EUVI. From EUV and soft X-ray (SXR) images we identify the erupting feature as a blowout coronal jet: in SXRs it is a jet with bright base, and in EUV it appears as an eruption of relatively cool ($\sim$ 50,000 K) material of horizontal size scale $\sim 30''$ originating from the base of the SXR jet. In SOT Ca II H images the most pronounced analog is a pair of thin ($\sim 1''$) ejections, at the locations of either of the two legs of the erupting EUV jet. These Ca II features eventually rise beyond $45''$, leaving the SOT field of view, and have an appearance similar to standard spicules except that they are much taller. They have velocities similar to that of "type II" spicules, ~ 100 km s^{-1}, and they appear to have spicule-like substructures splitting off from them with horizontal velocity ~ 50 km s^{-1}, similar to the velocities of splitting spicules measured by Sterling et al. (2010). Motions of splitting features and of other substructures suggest that the macroscopic EUV jet is spinning or unwinding as it is ejected. This and earlier work suggests that a sub-population of Ca II type II spicules are the Ca II manifestation of portions of larger-scale erupting magnetic jets. A different sub-population of type II spicules could be blowout jets occurring on a much smaller horizontal size scale than the event we observe here.

Subject headings: Sun: chromosphere — Sun: photosphere — Sun: magnetic fields — Sun: atmosphere — Sun: atmospheric motions

1. Introduction

Small-scale jet-like and explosive features at the solar limb are observed in a variety of wavelength bands. In chromospheric spectral lines, including Hα and Ca II, such features are generally referred to as spicules (Secchi 1877; Beckers 1968, 1972). Chromospheric spicules have long been noticed to be more extended in coronal hole regions, as first inferred by Rabin & Moore (1980) based on both their data and earlier observations. Larger-scale features similar to spicules are sometimes called macrospicules (e.g. Moore et al. 1977; Labonte 1979; Karovska et al. 1994). Jets of similar size scales are also observed at the solar limb at UV and EUV wavelengths, and are called UV- or EUV-spicules (e.g., Budnik et al. 1998; Wilhelm 2000; Xia et al. 2005; Pasachoff, Jacobson, & Sterling 2009) or macrospicules (with or without the wavelength adjectives) (e.g., Bohlin et al. 1975; Dere et al. 1989; Habbal & Gonzalez 1991; Parenti et al. 2002). Mariska (1992) and Sterling (2000) present additional general discussions of these features. Dynamic jets, usually on a larger scale, are also seen at soft X-ray (SXR) wavelengths, first by the *Yohkoh* spacecraft (e.g., Shibata et al. 1994; Shimojo et al. 1998); these features as called X-ray jets.

One of the key questions in spicule research is the nature of the relationship of the chromospheric spicules to the features seen at different wavelengths. Previous work shows that there is often a correspondence between features seen between chromospheric jets and UV or EUV spicules, as discussed observationally by Cook et al. (e.g., 1984) and Pasachoff et al. (2009) for spicules, and by Wang (1998) for macrospicules. One reason this question is important in the spicule case is because some spicules are reported to fade rather than obviously returning to the solar surface; for example Lippincott (1957) observed only 60% returning to the surface (also see discussions in Beckers 1968, 1972). If spicules undergo heating during their accent, then it is possible that they could fade from chromospheric wavelengths and reappear in UV or EUV wavelengths (Sterling & Hollweg 1984), which

would not only explain the fading, but also be a candidate for explaining the ultraviolet downflows revealed by redshifts in transition region lines (Pneuman & Kopp 1978).

The above discussion is all based on an earlier "era" of solar spicule research (Sterling 2000). There have been many advances over the last decade, fueled by higher-resolution ground observations, improvements in computational capabilities, and observations from space. Some examples of newer findings are the detection of very thin jet-like features called "straws" (Rutten 2006, 2007). De Pontieu et al. (2004) showed that photospheric p-mode oscillations are capable of explaining a category of spicules, going beyond earlier work on spicule wave models (e.g. Suematsu et al. 1982; Hollweg 1982; Sterling 2000), and Hansteen et al. (2006) showed that the mechanism is capable of explaining fibrils. Moreover, observations from the *Hinode* spacecraft are revolutionizing spicule studies to an even higher degree. De Pontieu et al. (2007) present evidence for two types of spicules seen in Ca II, with "type I" having velocities of a few $\times 10$ km s^{-1}, lifetimes of a few minutes, up-and-down motions along non-ballistic but parabolic paths, and appearing most prominently in more active solar locations. "Type II" spicules in contrast are characterized by higher velocities of 50—150 km s^{-1}, lifetimes of about one minute or less, and mainly upward-only motions followed by fading; they are prominent in coronal holes and quiet Sun, and perhaps also even in sunspot penumbra (Katsukawa et al. 2007). More recently, searches for the on-disk counterparts to the type II spicules have been fruitful, with (Langangen et al. 2008) and Rouppe van der Voort et al. (2009) identifying them with "rapid blueshifted events" (REBs). Sterling, Moore, & DeForest (2010) examined spicules at and near the limb in a polar coronal hole that apparently fall in the category of type II spicules, for clues to their origins and on how they disappear. The relationship between the formation mechanisms for type I and type II spicules, and the relationship between these types of spicules and the previously-studied "classical" spicules, are open questions.

Our understanding of X-ray jets also has been revolutionized by *Hinode* observations (e.g., certain et al. 2007; Savcheva et al. 2009). A basic physical mechanism seems to explain well the observations of many of the X-ray jets: emergence of a magnetic flux system into the corona where there is a pre-existing open field results in the jet when magnetic reconnection occurs between the two flux elements, with the jet extending along the open field (Yokoyama & Shibata 1995; Pariat et al. 2002). In an observational investigation, Moore et al. (2010) examined a large number of X-ray jets and determined that they can roughly be divided into two classes. One class they call "standard jets," which basically fit the emerging flux-open field reconnection picture. The second class they call "blowout jets," which begin as the standard jets do, but where the emerging bipolar flux loop or arcade erupts as the standard jet is being formed, resulting in a broader, "curtain-like" jet, along with the expulsion of cool chromospheric- and transition-region-temperature material in addition to the X-ray jet. These blowout jets have aspects analogous to larger-scale CME-producing magnetic eruptions, and make up about one-third of the X-ray jets in the Moore et al. (2010) survey. Because of their nature involving material ranging from chromospheric to coronal temperatures, these blowout jets have signatures in chromospheric, EUV, and coronal spectral channels; in contrast, the standard X-ray jets are most prominent in X-ray spectral channels and can have little or no signatures in cooler-temperature lines. Other work based on *Hinode* and other data also show a link between chromospheric, transition region, and coronal plasmas (e.g., De Pontieu et al. 2009; Mcintosh et al. 2009).

The aim of the current project is to identify an EUV jet in a polar coronal hole using data from the EUV Imaging Spectrometer (EIS) on *Hinode*, and find the counterpart to that EUV jet in other *Hinode* data, with the specific objective of learning about the relationship between the EUV feature and Ca II spicules, and about their signatures in SXRs. In the example we found, our observed EUV jet corresponded with what appears to

be a blowout X-ray jet. We report on these findings in the following.

2.   Data Set and Analysis Procedure

We use data from the *Hinode* satellite, supplemented with some images from the Solar Terrestrial Relations Observatory (*STEREO*) mission. *Hinode* carries three telescopes: the Solar Optical Telescope (SOT), which is a 50 cm white-light telescope/focal plane package (FPP) combination (Tsuneta et al. 2008); the EIS imaging spectrometer (Culhane et al. 2007); and the X-Ray Telescope (XRT; Golub et al. 2007).

Our data from SOT were obtained using the Ca II filter operating with 40 s cadence. This is too slow to see the detailed evolution of many of the typical type II spicules, which have lifetimes of 10—150 s according to De Pontieu et al. (2007). In addition to the standard SOT-processing routines, in their study of spicules Sterling et al. (2010) applied an image enhancement technique to the SOT images, whereby the SOT filtergraph images were convolved with the inverse point spread function (PSF) of the *Hinode* Ca II filter, where the PSF was deduced from eclipse measurements by C. E. DeForest via the methods of DeForest et al. (2009). (Also see Sterling & Moore 2010, for more details of the image processing procedure.) This improved the sharpness of the solar features, and also the contrast between the spicules and features on the disk just inside the limb (the features called "Ca II brightenings" by Sterling et al. 2010). For the current study we analyzed our data both applying and omitting this technique. Because the convolution procedure can introduce a graininess to some of the images, we find that in some cases, especially when looking off the limb, the non-convolution-processed images have an advantage over the convolution-processed images for our current study, and the results we present here are the non-convolution-processed images. In this study we applied a radial filter (using a version developed by T. Berger, and available in the solarsoft software package) to the features

inside the limb and to the brightest spicules. Adjusting the parameters of this filter allows us to make intensities of all the features of interest about the same, improving the overall visibility of all the features because of the resulting more-limited dynamic range of the images.

EIS can operate in several modes. For the data examined here the study named "assignment_266" was run, which consists of a sequence of images taken with the 266″-wide EIS slit, referred to as a "slot," with the slot oriented in the north-south direction with a height of 512″, and with 1″ pixels. (See, e.g., Ugarte-Urra, Warren, & Brooks 2009, for more information on EIS slot data). This study was designed for quiet Sun observations in the "sit and stare" mode, i.e., without rastering of the image, covering five wavelength bands: Fe XII, Fe XIII, He II, Si X, and Fe XV, taken simultaneously and with a cadence of 124 s. These are excellent characteristics for identifying EUV jets with EIS. We cannot assume however that EUV spicules per-se are resolvable, since the widths of chromospheric spicules from ground measurements are typically $< 1″$ (Beckers 1968; Nishikawa 1988; Pasachoff et al. 2009), and *Hinode* Ca II spicules have been observed to be much narrower still, down to the resolution limit of ~ 150 km or less for some of them (De Pontieu et al. 2007; Sterling et al. 2010).

Our XRT data are from two of the instrument's thinner filters, the "Ti-poly" and the "Al-mesh" filters, which are sensitive to plasmas hotter than from ~ 1 MK. XRT's CCD has 1″ pixels, and therefore its resolution is comparable to that of EIS, and the cadence of our data is 6 min for each filter. For our studies, both filters show the features we are interested in; namely, they both show evidence for and the nature of an X-ray jet corresponding to the features that we see in the field of view (FOV) of both SOT and EIS, and so our detailed discussions are based on results from the Ti-poly filter only. *STEREO* consists of a pair of satellites at 1 AU, one ahead of (*STEREO* A) and one behind (*STEREO* B) the Earth in

its orbit, providing two different viewing angles of the Sun; at the time of our observations of this study however, the two were only 3 degrees apart. Both *STEREO* satellites have EUV telescopes (SECCHI/EUVI) with four filters tuned to wavelengths 304 Å, 171 Å, 195 Å, and 284 Å. We use these data to supplement the *Hinode* observations, both because of the additional wavelength coverage afforded by *STEREO*, and because the event that is our main focus of our investigations began some minutes before *Hinode* began to observe it, and the *STEREO* data therefore show us what was happening prior to when the *Hinode* observations commenced.

We first searched for jets in EIS EUV data, because identifying jets in EIS with good cadence requires specific operation modes, such as slot images taken at a rapid cadence when pointed at the limb. Generally the jets appeared best in the EIS He II channel. After identifying candidate EIS jets, we then checked to see whether SOT, which often operates with a substantially more limited FOV than the wide EIS slot, was observing the solar polar limb and taking appropriate Ca II images. Finally, we checked to see whether XRT was taking data appropriate for our study. When a candidate EIS jet met these criteria, we checked to see whether SOT was observing in Ca II with adequate time cadence, and if the candidate EIS feature was in the SOT FOV. Even when jets satisfied these criteria, we later found cases where the SOT FOV covered mainly the solar disk with $\lesssim 10''$ of the off-disk Sun in the SOT FOV to be not suitable for our study, because it was virtually impossible to discern any signature of the EIS event in the SOT data. Without a clear corresponding feature in the two data sets, it would be extremely difficult to adjust the alignment between the EIS and SOT data to the required accuracy; although the EIS coarse mirror was moved on 2007 January 30 in order to minimize the offset between EIS and SOT, we wanted to identify the same feature in both instruments in order to finalize the alignment. Moreover, in addition to the intrinsic residual mis-alignment between the two instruments, the pointing of the SOT filtergraph images undergoes a drift with time due to the gross motion of solar

granules seen over a narrow field of view used for image stabilization (Shimizu et al. 2007), and this drift can be accentuated when observing near the limb. These and other motions necessitate a final tweaking of the alignment between data in the various instruments, which we wanted to do by identifying corresponding features. The data set we settled on for this current study had the SOT FOV positioned so that several tens of arcsec beyond the limb were visible in the SOT FOV. As we will show below, in this case a feature was visible in SOT Ca II that coincides with the precise timing of the EIS object, making it possible to carry out an accurate alignment adjustment. In retrospect, this experience made it clear why we had trouble identifying a signature of the EIS jet in the SOT data in the cases where there the SOT FOV was not positioned to see far enough off the solar limb: within $\sim 10''$ of the limb, the Ca II emission is dominated by the forest of spicules, and the object corresponding to the EIS jet in our example is indistinguishable from the standard spicules in the forest at those heights. For the EIS jet we observe however, the corresponding Ca II feature extends well above the spicule forest, and so a positive cross-identification becomes possible. This event began on 2007 April 1, near 00:09 UT, based on data from *STEREO*. *Hinode* had just completed a pointing maneuver to observe the north polar limb near this time, and the first image in EIS was at 00:12:21 UT, the first SOT Ca II image was at 00:15:35 UT, and the first XRT Ti-poly image was at 00:15:25 UT. Therefore we are not able to follow the origin of the event in *Hinode* data, but we are able to see the evolution of the Ca II and SXR structures corresponding to the EIS jet from shortly after its onset.

3. Observations

3.1. Observations in EUV and SXRs

Figure 1 shows the erupting feature in EUV in SXRs. Figures 1a—1c show three images from the EIS 256 Å He II channel; these are frames from a video accompanying

the online version of this paper. This EIS channel contains some blends with coronal lines, and so it is not a "pure" channel, but at least on the surface the majority of the emission is from material of ∼50,000 K (Young et al. 2007), which might be considered upper chromosphere or transition region-material; above the limb coronal emission tends to dominate the the EIS 256 Å channel. In panel (a) there are three clear brightenings, with the two eastern-most brightenings apparently connected by fainter emission and resembling a loop structure, and with the entire bright complex having a horizontal size of $\sim 30''$. By the time of panel (b) the entire complex appears connected by a faint loop, while there is material ejected from the east side of the structure extending vertically out of the frame. By the time of panel (c) the whole structure has faded, but there is still emission extending vertically from the location of the original low-lying complex. Panels (d)—(f) show the same EIS 256 Å images as in the first three panels, but with intensity contours drawn over a restricted region of the FOV. Below in Figure 3 we will plot similar contours to indicate the alignment between the EIS and the SOT Ca ɪɪ images.

Figures 1a—1f show a subsection of the full EIS slot images, but from a movie made from those full slot images we can measure the velocity of the outward-moving feature between the frames. Over 00:12:21 UT—00:14:25 UT we find the velocity to be $\sim 225 \pm 50$ km s^{-1}, and over 00:12:21 UT—00:16:29 UT the velocity is $\sim 175 \pm 15$ km s^{-1}; our estimated uncertainty is lower in this second pair of frames because a distinct feature can be identified at both times, but the top of the ejection is more broadly distributed in the 00:14:25 UT image. The velocity over the time period 00:14:25 UT—00:16:29 UT is also of interest since it can more directly be compared with the features seen in SOT discussed below; we find that velocity to be $\sim 130 \pm 50$ km s^{-1}.

The last two rows in Figure 1 show coronal emission. Panels (g)—(i) are from the EIS 284 Å channel, which has a peak response of around 2 MK (Young et al. 2007).

Panels (i)—(k) are images from the XRT Ti-poly filter, which has a strong response to plasmas in excess of a few MK (Golub et al. 2007). There are two arcade structures visible along the line of sight. One of these is an arcade at the limb, with coordinates of about (30,960), and a second arcade structure is in the foreground at coordinates (40,950). The background structure is on the limb and is brightest in the three XRT images (panels j-l), and somewhat dimmer but of roughly constant brightness in the three EIS 284 Å images (panels g—i). This background feature is markedly faint or absent in the EIT 256 Å images in panels (a—f), indicating that this background structure is a very high-temperature arcade compared to the feature that is visible in the EIS 256 Å images. From the hotter-line images of panels (g)—(l), next to the bright compact "foreground" arcade to the west pointed out by the upward-pointing arrow in Figure 1j, there is a vertical curtain-like sheath of emission pointed out by the horizontal arrow in Figure 1j. Thus this set of coronal images (Figs. 1g—1l) shows a curtain-like jet structure being ejected.

As noted in §1, Moore et al. (2010) discussed two different types of coronal X-ray jets: standard jets and blowout jets. As shown in the cartoon of our Figure 2, which is a repeat of Figure 10 in Moore et al. (2010), the setup for a both types of jets consists of a compact emerging magnetic coronal arcade structure that emerges into a pre-existing "open" field. There is a magnetic neutral line surrounding one base of the emerging arcade, the positive base in the cartoon of Figure 2, because that arcade is embedded in the mainly-monopolar coronal hole field, which is shown as negative polarity in Figure 2. Along the base of the positive side of the emerging arcade, there is a current sheet between that emerging arcade and the open field. Eventually, magnetic reconnection occurs at this current sheet, creating two magnetic reconnection products, one of which is the X-ray jet (see caption to Fig. 2). If the resulting jet is a "standard" X-ray jet (that is, not a blowout jet), then the process would end shortly after the time of Figure 2b, with a bright X-ray loop (arcade) over the west-side neutral line below the reconnection X-point, and an X-ray jet whipping out of the top side

of the reconnection X-point. After the field relaxes down to the Figure 2a configuration, the standard X-ray jet eruption process would have finished; most significantly, the emerging arcade to the east of the new reconnection loop in Figure 2b would remain stable. (Fig. 1 of Moore et al. 2010, describes this standard jet eruption process in more detail.) In this case, only a very small volume of chromospheric-temperature material ends up being ejected, and the eruption is strongly prominent in SXRs but weak in EUV, from the findings of Moore et al. (2010).

In the blowout jet case however, the emerging arcade east of the new reconnection loop of Figure 2b does not remain stable. Rather, it becomes destabilized by the earlier dynamics, and the entire emerging arcade sitting east of the initial reconnection point in Figure 2b erupts, as depicted in Figure 2c. When this erupting bipole is small enough, roughly $\lesssim 30''$ according to Moore et al. (2010), it carries substantial quantities of chromospheric- and transition-region-temperature material with it, resulting in enhanced emission in chromospheric and EUV lines. Also, this erupting bipole reconnects with the vertical field during the eruption (crosses in Fig. 2c), and that can result in an X-ray jet of a substantially larger horizontal size span than in the case of the standard X-ray jet, and results in a curtain-like appearance of the jet. By the time of Figure 2d, the X-ray jet is narrowing, as the whole system subsequently relaxes down to the initial state of Figure 2a. (Moore et al. 2010, describe the blowout jet eruption process in more detail.)

Our event of Figure 1 displays characteristics of a blowout jet. Its overall size is relatively compact, with the base of the entire feature only spanning about $30''$, or about 20,000 km, and this is consistent with the primary loop structures involved being largely or completely contained inside of the chromosphere. In SXRs, the brightest feature is on the west end of the full structure, at the location of the upward-pointing arrow in Figure 1j, and extending to the east of (and maybe somewhat behind) this is a curtain of SXR emission

jetting upward. The upward-pointing arrow would correspond to the small loop on the west side of the cartoon in Figure 2b, while the curtain-like jet would correspond to field opening above the eruption of the large arcade to the east in the cartoons of Figures 2c and 2d. Unfortunately the *Hinode* observations did not begin until the jet structure was already developed, and it is visible in a fully-developed curtain-like form in only one of the XRT frames, which is shown in Figure 1j. *STEREO* however, for example in 171 Å images, shows the presence of a plume at the location of the curtain of emission in XRT, and those images also show a brightening of the base of the plume at 00:11:30 UT and continuing until at least 00:26:30 UT on 2007 Apr 1, fully consistent with the formation of an X-ray jet at the time of the XRT image in Figure 1j. This corresponds to the situation and the orientation of the cartoon of Figure 2c and 2d, with the compact arcade on the west side and the curtain-like jet to the east. At the time of Figure 1j the compact arcade is very bright compared to the jet, and the same tendency occurred in the example blowout jets of Moore et al. (2010). Hot EUV emission from the EIS 284 Å images of Figure 1g and 1h show similar features, with the jet and arcade dim or invisible by the time of Figure 1i. Moreover, the image in Figure 1a from the He II 256 Å channel is consistent with an arcade of relatively cool chromospheric or transition region material exploding to the east of the bright SXR and 284 Å feature, and the material continuing to erupt as a jet in Figures 1b and 1c; this corresponds to the cartoon in Figure 2c. The arcade corresponding to the flare arcade over the emerging flux in the cartoon, that is the red loops in the east of Figures 2c and 2d, may correspond to the bright background arcade at the limb in the coronal emission of Figures 1g—1l. It is hard to be certain of the geometry of the setup however due to the near-limb perspective, and because the two *STEREO* spacecraft were only separated by 3° on the date of this event.

In the full-sized EIS 284 Å slot images, we can see that the jet of Figure 1g is already at least 60″ tall in that first image at 00:12:21 UT, and moves with an average velocity of

~ 120 km s^{-1} between then and the time of the next frame at 00:14:25 UT, although with a large uncertainty. In the first XRT image, at 00:15:25 UT, the jet already extends to essentially the edge of the full frame FOV, $\sim 240''$ above the surface, and the jet is hard to distinguish from a plume in that single frame. By the time of the next XRT frame, at 00:21:25 UT, the jet has faded substantially, and so it is not possible to estimate a velocity of the X-ray jet in the XRT images.

3.2. Observations in Ca II

We have observed a jet eruption in a coronal hole at the solar pole in EUV, and we have established that this corresponds to an X-ray jet seen in XRT. Moreover, we have good evidence that the coronal jet is of the blowout variety, according to the classification of Moore et al. (2010). We want to know what this feature looks like in Ca II, and in particular how it might manifest itself in terms of a Ca II spicule or group of spicules.

Figure 3 shows the results of our concurrent observations with SOT, panels (a)—(c) of which are frames from an video accompanying this paper. The figure shows the typical spicule forest, extending to about $10''$ above the surface. Extending greatly beyond this however is the structure corresponding to the eruption seen in EIS and XRT. In the bottom row of Figure 3, we show the same images as in the top row, but with the EIS 256 Å contours of Figures 1d and 1f overlaid onto Figures 3d and 3f; because the EIS observations started earlier than the SOT observations, the EIS contour of Fig. 1e best matches the time of the SOT image in Figs. 3a and 3d, and so Fig. 3e uses an EIS contour not shown in Fig. 1 (the EIS 256 Å image corresponding to the contour of Fig. 3e however is in the video accompanying Fig. 1a—1c). We did a fine-tuning adjustment to the alignment of the SOT and EIS images, as discussed in §2, using the limb of the Sun and the position of the EIS contours on the SOT images. Both the horizontal extent of the feature, and the vertical

extent of the feature at different times, correspond well with the EIS features, where we have matched the times as closely as possible; the EIS data started earlier than the SOT data, and so the difference in times between the SOT image and the EIS contours is 194 s in panel (d), but the time differences are only 18 s and 21 s in panels (e) and (f), respectively. When the intensity of the above-the-limb features is pumped up and processed, as is the case here, and with the foreknowledge that we are looking at a feature corresponding to a jet in EUV and SXRs, it is obvious that the Ca II features are part of a larger macro-structure. Without the extra processing and foreknowledge however, these features could be mistaken for two or more separate, very tall spicules being ejected independently of each other. We refer to the two most prominent spicule-like features as the "east spicule" and the "west spicule." (There is a semantics question of whether features of such great height beyond the spicule forest should be referred to as "spicules," but we will bypass that discussion in this paper.) We find that the west spicule has a velocity of 110 ± 10 km s^{-1} measured over 00:16:11 UT to 00:17:31 UT, and the east spicule has a velocity of 125 ± 5 km s^{-1} measured over 00:16:51 UT to 00:18:11 UT. These values are similar to that of the EIS 256 Å jet of 130 ± 50 km s^{-1} measured over 00:14:25 UT to 00:16:29 UT, and also typical of type II spicules as measured by De Pontieu et al. (2007) and by Sterling et al. (2010).

Figure 4 shows the Ca II ejection in more detail, showing the structure's development and eventual fading with time. These frames are of particular interest when compared with the video (see video corresponding to Fig. 3), in that the video gives the impression of a splitting of the east spicule, as shown by the arrows pointing to the left in panels (d)—(f). The splitting-off feature moves westward with a velocity of 50 ± 10 km s^{-1}, and this value is typical of the splitting velocities found by Sterling et al. (2010). Spicule-like features near the west spicule also show what appears to be splitting, although not as clearly as the east spicule. The arrows pointing to the right in Figures 4e and 4f point out one such feature that appears to move west to east; its motion seems more complex than a simple constant

eastward flow, and so we do not quote a velocity value for that feature here.

4. Summary and Discussion

We have obtained one answer to the question of what the counterpart of an EUV jet is in chromospheric emission, which is one of the questions posed by Sterling (2000) for spicule research in the *Hinode* era. In EUV we observed what we can now identify as a blowout coronal jet, according to the description of Moore et al. (2010). That paper argues that blowout jets include destabilization and ejection of material at upper-chromospheric and transition region temperatures, in the form of a small-scale ($\lesssim$20,000 km) arcade or loop, frequently with a corresponding hotter X-ray jet. Our data in EUV from EIS and *STEREO*, and in SXRs from XRT, are consistent with this picture.

In Ca II images from SOT of the chromosphere, we find that the blowout jet produced two bright spicule-like features, one on either side of the erupting EUV arcade. These two features both had velocities comparable to those measured elsewhere for type II spicules. The situation is more complex than two single individual spicule-like features however, because both spicule-like features belong to the same macroscopic structure, and therefore the two features are to some degree coordinated in their movements and lifetimes. The two features extend to heights greater than 45″ (the edge of the SOT FOV), and in fact some of the material apparently flows out the top of the SOT FOV. In addition, the region in-between those east and west spicules contains spicule-like dynamic substructure. The substructure is similar to the detailed structure of solar prominences (e.g., Berger et al. 2008). The east and west spicules apparently reside on the legs of the exploding blowout loop (arcade in three dimensions), and some of the substructure could result from the multiple locations of magnetic reconnection expected to be present, as indicated by the multiple reconnection x-points in Figure 2c. Scullion et al. (2009) have also mapped strong

jet-like events to cool features that may be spicules, and those could be similar to the hot material-cool material connections we find here.

Sterling et al. (2010) observed several cases where spicules appeared to start their rise as a single structure, and then split into two or more structures. We observed a similar phenomenon here, most clearly with the east spicule having another structure move away from it to the west at ~ 50 km s^{-1}, similar to the velocities observed by Sterling et al. (2010). This motion is toward the interior of the macroscopic erupting blowout jet, and one possible explanation for the horizontal motions is that the macroscopic structure is rotating; we also see motions of substructure in the west-to-east direction (Fig. 4e—4f), which would be expected in addition to the east-to-west motions in the case of rotation. In the scenario pictured in Figure 2, a spinning of the open field line structure could conceivably be induced by the exploding arcade at the base to the east in the figure, if that exploding arcade had pre-existing twist. In that case, the twist would be induced onto the open field lines when the twisted exploding arcade reconnected with the open field in order to conserve helicity, and subsequently the open field would be able to unwind. In our data we cannot discern twisting motions in, for example, the EUV 256 Å images, but that could be due to the small size of the object combined with the 1″-pixel resolution of EIS, or the coarseness of the cadence, in this case. Nonetheless, other erupting jets have been observed to rotate (e.g., Pike & Mason 1998).

It is unclear how common splitting spicules may be. Sterling et al. (2010) listed seven events observed in a 70 min movie viewing 30″ of the polar coronal hole, during which time hundreds of more standard spicules would have occurred. But they may only have been able to identify the most obvious features, such as ones that were unusually tall or otherwise stood out from the standard background spicules. If splitting spicules are relatively faint and occur while in the haze of many surrounding spicules, then it could be

hard to recognize the splitting, and so it is hard to know the occurrence rate. In the case discussed here, the blowout eruption seen in EIS and XRT spans ~20,000 km, and produces Ca II spicule-like objects with lengths in excess of 30,000 km and with lifetimes of ~ 5 min or more, quite different from most type II spicules, which tend to live about one minute or less, and have much shorter heights. So if the east- and west-spicule features we observe here are type II spicules, then they are not typical ones. Sterling et al. (2010) did however observe a pair of coordinated features, namely events 6 and 7 in their Table 2. Those two events had velocities of ~ 130 and 70 km s^{-1}, only reached heights of ~ 5000 km, and had lifetimes of ~ 90 s, which are much more typical numbers for type II spicules. Those objects had a separation of only 1500 km, and therefore they could have been been a scaled-down version of the event we present here. That is, the pair of spicules of this paper are part of a macroscopic structure, namely a blowout coronal jet, of size-scale 20,000 km, while the spicule events 6 and 7 of Sterling et al. (2010) Table 2 may also be part of a macroscopic feature, but of size-scale ~ 1500 km.

In itself, our observation of spicule-like counterparts to a blowout eruption does not give direct insight into the actual spicule-producing mechanism. Our east- and west-spicules are a byproduct of a larger-scale explosive eruption (the blowout jet), and they would have to be created on relatively isolated portions of the overall exploding magnetic blowout jet, or on portions of the vertical field with which the exploding magnetic structure of the blowout jet undergoes magnetic reconnection. A possibility is that such reconnections could deposit energy in the chromosphere, leading to ejective outflows along the field. Shibata et al. (1982) explored the concept of the response of the atmosphere to energy deposition in the chromosphere. Sterling et al. (1991) and Sterling, Shibata, & Mariska (1993) did similar studies in more thermodynamic detail, and found that spicule-like features could develop in some cases. Simulations by Heggland, De Pontieu, & Hansteen (2009) support that wave-induced reconnection can produce spicule-like features in some circumstances.

Suematsu et al. (2008) describe observations of a double-thread structure in more than 50% of the spicules they studied. This is similar to the finding of Tanaka (1974) that $\sim 30\%$ of mottles can be resolved into a double structure under high resolution. Sterling et al. (2010) suggested that the splitting spicules could be responsible for the double structures seen in those earlier observations. Another possibility however is that the two spicules bounding a macroscopic erupting structure, that is, features like the east- and west-spicules of this paper, and probably the events 6 and 7 of the Sterling et al. (2010) paper, might be what was observed as a double structure by Suematsu et al. (2008) and Tanaka (1974). This possibility requires that the "macroscopic structure," i.e. the feature corresponding to the blowout coronal jet in the event of this paper, be scaled down to much smaller sizes than what we observed here and in Sterling et al. (2010), and in that case the spicule itself would be a miniature magnetic eruption. The possible spinning of our structure, as suggested by the counter-directional horizontal motions of spicule-like filamentary structures in Figure 4, is also consistent with the suspected spinning of some of the double spicules of Suematsu et al. (2008). Moreover, from some time ago the tilts of spectral lines of spicules have been suggested as evidence for the twisting motions of spicules (Pasachoff, Noyes, & Beckers 1968).

The idea of a scaled-down magnetic eruption producing spicules was introduced before (Moore et al. 1977; Moore 1989, 1990, 2001, e.g.,). In order for a substantial portion of the type II spicules to be magnetic eruptions, what would be required is small bipoles of size ~few arcsec emerging in large numbers in "open" magnetic field regions. Observations from *Hinode* (e.g., Orozco Suárez et al. 2007; Lites et al. 2008; Ishikawa & Tsuneta 2009a,b; Ishikawa et al. 2010) and earlier (e.g., Lites et al. 1996), show that an abundance of transient horizontal field is present in the photosphere of the size scale of granules, of flux of perhaps ~ 400 G and lifetimes of 1—10 min, and these could possibly be the source for some such spicules. In addition, Schrijver (2010) shows that eruptions of bipoles occur with

increasing frequency as their size decreases, from the largest CMEs down to bipolar regions of a few arcseconds in size. Eruptions creating spicules may be at small end of this size scale, or smaller still.

Should many of the type II spicules in open field regions be due to magnetic eruptions, then it is conceivable that the spicules could fuel the fast solar wind if only a small percentage of their mass escapes solar gravity (Pneuman & Kopp 1978) (and assuming previous mass determinations for spicules applies to type II spicules). De Pontieu et al. (2009) combine Ca II images from SOT with spectral information from EIS and from the SUMER instrument on SOHO to obtain strong evidence that the solar wind originates from open field regions populated by type II spicules. Similarly, Mcintosh et al. (2010) find evidence from STEREO observations that jets in plumes are responsible for the solar wind there. Either the same or similar processes could occur at the boundary between closed active region fields and open coronal hole fields, which Sakao et al. (2007) demonstrated is a solar wind source location using data from XRT, supported by observations by Harra et al. (2008) with data from EIS. These solar wind studies could be consistent with the concept of some spicules being miniature blowout jets.

REFERENCES

Beckers, J. M. 1968, Sol. Phys., 3, 367

Beckers, J. M. 1972, ARA&A, 10, 73

Berger, T. E., et al. 2008, ApJ, 676, L89

Bohlin, J. D., Vogel, S. N., Purcell, J. D., et al. 1975, ApJ, 197, L133

Budnik, F., Schroder, K.-P., Wilhelm, K., & Glassmeier, K.-H. 1998, A&A, 334, L77

Cirtain, J. W. et al.2007, Science, 318, 1580

Cook, J. W., Brueckner, G. E., Bartoe, J.-D. F., & Socker, D. G. 1984, Adv. Space Res. 4, 59

Culhane, J. L., Harra L. K., James, A. M., et al. 2007, Sol. Phys., 243, 19

DeForest, C. E., Martens, P. C. H., & Wills-Davey, M. J. 2009, ApJ, 690, 1264

De Pontieu, B., Erd'elyi, R., & James, S. P. 2004, Nature, 430, 536

De Pontieu, B., et al. 2007, PASJ, 59, S655

de Pontieu, B., McIntosh, S. W., Hansteen, V. H., & Schrijver, C. J. 2009, ApJ, 701, L1

Dere, K. P., Bartoe, J.-D. F., Brueckner, G. E., & Recely, F. 1989, ApJ, 345, L95

Golub, L., Austin, G., Bookbinder, J., et al. 2007, Sol. Phys., 243, 63

Habbal, S. R. & Gonzalez, R. D. 1991, ApJ, 376, L25

Hansteen, V. H., De Pontieu, B., Rouppe van der Voort, L., van Noort, M., & Carlsson, M. 2006, ApJ, 647, L73

Harra, L. K. et al. 2008, ApJ, 676, L147

Heggland, L., De Pontieu, B., & Hansteen, V. H. 2009, ApJ, 702

Hollweg, J. V. 1982, ApJ, 257, 345

Ishikawa, R. & Tsuneta, S. 2009a, A&A, 495, 607

Ishikawa, R. & Tsuneta, S. 2009a, in ASP Conf. Ser. 415, The Second Hinode Science
     Meeting: Beyond Discovery-Toward Understanding, ed. B. Lites et al. (San Francisco,
     CA: ASP), 132

Ishikawa, Tsuneta, & 7 Jurčák 2010, ApJ, 713, 1310

Karovska, M., & Habbal, S. 1994, ApJ, 431, L59

Katsukawa, Y., et al. 2007, PASJ, 59, S577

LaBonte, B. J. 1979, Sol. Phys., 61, 283

Langangen, O, De Pontieu, B., Carlsson, M., Hansteen, V. H., Cauzzi, G., & Reardon, K.,
     ApJ, 2008, 679L, 167

Lippincott, S. L. 1957, Smithsonian Contrib. Astrophys., 2, 15

Lites, B. W., Leka, K. D., Skumanich, A., Martinez Pillet, V., & Shimizu, T. 1996, ApJ,
     460, 1019

Lites, B. W. et al. 2008, ApJ, 672, 1237

Mariska, J. T. 1992, The Solar Transition Region, Cambridge University Press, New York

McIntosh, S. W., & De Pontieu, B. 2009, ApJ, 707, 524

McIntosh, S. W., Innes, D. E., de Pontieu, B., & Leamon, R. J. 2010, A&A, 510, L2

Moore, R. L., Tang, F., Bohlin, J. D., & Golub, L. 1977, ApJ, 218, 286

Moore, R. L. 1989, in Solar System Plasma Physics, ed. J. H. Waite, J. L. Burch, & R. L. Moore (Washington, DC: AGU), 1

Moore, R. L. 1990, Memorie della Societa Astronommica Italiana, 61(2), 317

Moore, R. 2001, in Encyclopedia of Astronomy and Astrophysics, ed. P. Murdin (Bristol: Inst. of Phys. Publ.), 2691

Moore, R. L., Certain, J. W., Sterling, A. C., & Falconer, D. A. 2010, ApJ, submitted

Nishikawa, T. 1988, PASJ, 40, 613

Orozco Suárez, D. et al. 2007, ApJ, 670, L61

Parenti, S., Bromage, B., & Bromage, G. E. 2002, A&A, 384, 303

Pariat, E., Antiochos, S. K., & DeVore, C. R. 2010, ApJ, 714, 1762

Pasachoff, J. M., Noyes, R. W., & Beckers, J. M. 1968, Sol. Phys., 5, 131

Pasachoff, J. M., Jacobson, W. A., & Sterling, A. C. 2009, Sol. Phys., 260, 59

Pike, C. D. & Mason, H. E. 1998, Sol. Phys., 182, 333

Pneuman, G. W. & Kopp, R. A. 1978, Sol. Phys., 57, 49

Rabin, D. & Moore, R. L. 1980, ApJ, 241, 394

Rouppe van der Voort, L., Leenaarts, J., De Pontieu, B., Carlsson, M., & Vissers, G. 2009, ApJ, 705, 272

Rutten, R. J. 2006, Proceedings 23th NSO Workshop (ASP Conf. Ser. 354), ed. J. Leibacher, R. F. Stein, & H. Uitenbroek (San Francisco, CA: ASP), 276

Rutten, R. J. 2007, The Physics of Chromospheric Plasmas (ASP Conf. Ser. 368), ed. P. Heinzel, I. Dorotovic, & R. J. Rutten (San Francisco, CA: ASP), 27

Sakao, T. et al. 2007, Science, 318, 1585

Savcheva, A., Cirtain, J. W., Deluca, E. E., & Golub, L. 2009, ApJ, 702, L32

Scullion, E., Popescu, M. D., & Banerjee, D., et al. 2009, ApJ, 704, 1385

Schrijver, C. J. 2010, ApJ, 710, 1480

Secchi, P. A. 1877, Le Soleil. Gauthiers-Villars, Paris, Vol. 2, Ch. lI, §1

Shibata, K., Nishikawa, T., Kitai, R., & Suematsu, Y. 1982, Sol. Phys., 77, 121

Shibata, K., Yokoyama, T., & Shimojo, M.NRO Rep. 1994, New Look at the Sun with Emphasis on Advanced Observations of Coronal Dynamics and Flares, Vol. 360, ed. S. Enome & H. S. Hudson (Tokyo: National Astronomical Observatory of Japan), 75

Shimizu, T., et al. 2007, PASJ, 59, S845

Shimojo, M., Shibata, K., & Harvey, K. L. 1998, Sol. Phys., 178, 379

Sterling, A. C. 2000, Sol. Phys., 196, 79

Sterling, A. C., & Hollweg, J. V. 1984, ApJ, 285, 843

Sterling, A. C., & Hollweg, J. V. 1988, ApJ, 327, 950

Sterling, A. C., Mariska, J. T., Shibata, S., & Suematsu, Y. 1991, ApJ, 381, 313

Sterling, A. C., Shibata, K., & Mariska, J. T. 1993, ApJ, 407, 778

Sterling, A. C., Moore, R. L., & DeForest, C. E. 2010, ApJ, 714, L1

Sterling, A. C., & Moore, R. L. 2010, Proceedings to the Third Hinode Science Meeting, Tokyo 2009. In press.

Suematsu, Y., Shibata, K., Nishikawa, T., & Kitai, R. 1982, Sol. Phys., 75, 99

Suematsu, Y., et al. 2008, ASP Conference Series, 397, 27S

Tanaka, K. 1974, in IAU Symp. 56, Chromospheric Fine Structure, ed. R. G. Athay (Boston: Reidel), 239

Tsuneta et al. 2008, Sol. Phys., 249, 167

Ugarte-Urra, I., Warren, H. P., & Brooks, D. H. 2009, ApJ, 695, 642

Wang, H. 1998, ApJ, 509, 461

Wilhelm, K. 2000, A&A, 360, 351

Xia, L. D., Popescu, M. D., Doyle, J. G., & Giannikakis, J. 2005, A&A, 438, 1115

Young, P. R. et al. 2007, PASJ, 59, 857

Yokoyama, T. & Shibata, K. 1995, Nature, 375, 42

Fig. 1.— Erupting jet viewed in different wavelengths. Panels (a)—(c): EIS 256 Å He II images, showing upper-chromosphere or transition region material being ejected as an EUV jet. Panels (d)—(f): Same as (a—c), but with selected intensity contours overplotted, for comparing with SOT images in Fig. 3. Panels (g)—(i): Frames from the EIS 284 Å Fe XV channel, showing coronal material. There are two arcade structures visible, one in the foreground centered at about (40,950) that fades by the time of panel (i), and one in the background at about (30,960) that remains bright throughout all three frames. Panels (j)—(l): Frames from XRT, showing hot coronal material. In (j), the upward-pointing arrow shows the foreground feature of panels (g—i), and the horizontal arrow shows a curtain-like SXR jet positioned where the EUV eruption of (a—f) occurs. Taken together, the images in this figure suggests that the jet has the form of a blowout coronal jet, as described by Moore et al. (2010). For this and all solar figures in this paper the color table is reversed, so that Ca II brightenings on the solar disk appear dark. North is up and West is to the right in this and all other figures of this paper. (An animation of panels (a)—(c) are available in the online journal.)

Fig. 2.— Cartoons showing schematics of a blowout coronal jet, reproduced from Moore et al. (2010). (a) Magnetic setup prior to onset of coronal jet eruption. A bipolar arcade sits beneath open field that is anchored in negative polarity. A current sheet, represented here as the short solid-line black curve on the west (right) side of the panel, is starting to form between the bipole and the open field. In (b), magnetic reconnection has occurred at the location of the current sheet, now an x-point represented by the black cross. The small red loop on the west side and the red field line anchored on the east side are newly-formed products of the reconnection, with the latter forming an X-ray jet. If the magnetic bipole remains stable through the process, then the jet-formation process would end shortly after this time, with the setup relaxing down to the configuration of (a). (c) In the case that the process in (b) leads to an instability of the magnetic bipole, the bipole erupts outward,

resulting in magnetic reconnection between the erupting bipole and the overlying negative-polarity open field at several locations, indicated by the two higher black crosses, and also resulting in "internal reconnection" between the legs of the erupting bipole, indicated by the lowest of the three black crosses. These reconnections result in a broadening to the size scale of the entire magnetic structure of the jet that was relatively narrow in (b), so that the jet takes on a curtain-like structure, and in additional brightening and growth of the loop in the west that was smaller in (b). The internal reconnection makes a flare arcade (red loops in the east) over the inside neutral line in (c) and (d), making the inside of the erupting bipole bright in coronal X-ray and EUV emission. (d) At later stages the jet narrows as the erupting field becomes stretched out and the entire structure begins to relax down to the configuration of (a). The erupting loop of Figs. 1a—1f corresponds to the eruption of the bipole in (c), and Fig. 1j corresponds to the well-developed curtain jet of (c), with the horizontal arrow in Fig. 1j corresponding to the curtain jet and the vertical arrow in Fig. 1j corresponding to the reconnection-product arcade represented by the relatively small red loops on the west side of (c).

Fig. 3.— (a)—(c): Sequence of frames showing the eruption in SOT Ca II H images, where a radial filter has been applied to the photosphere and to the spicule forest, to show better the Ca II features corresponding to the EUV and SXR eruption. The most prominent features are two growing Ca II spicule-like objects, which we refer to as the east- and west-spicules in this paper. (d)—(f): Same as (a—c), but with the EIT 256 Å He II contours from Figs. 1d and 1f overlaid onto (d) and (f), respectively, showing the correspondence between the EUV jet and Ca II features. (Fig. 3e uses an EIS 256 Å contour closer in time to the SOT image of Fig. 3b, than the contour of Fig. 1e.) The east- and west-spicules correspond to the legs of the erupting jet, best seen in Figs. 1c and 1f. Horizontal striations in intensity in the images are an artifact of the radial filter. (An animation of panels (a)—(c) are available in the online journal.)

Fig. 4.— Time series of a closeup of the SOT Ca II H feature of Fig. 3, corresponding to the EUV and SXR jet of Fig. 1. Arrows pointing to the left in (d)—(f) show a feature that appears to be splitting off from the east spicule. Similarly, arrows pointing to the right in (e) and (f) show a feature that has rather complex motions, but generally appears to be moving from west to east. Taken together, the two features pointed out by the arrows, and other similar moving features apparent in the movie, suggest that the entire macro-structure may be rotating or unwinding as the blowout jet erupts.
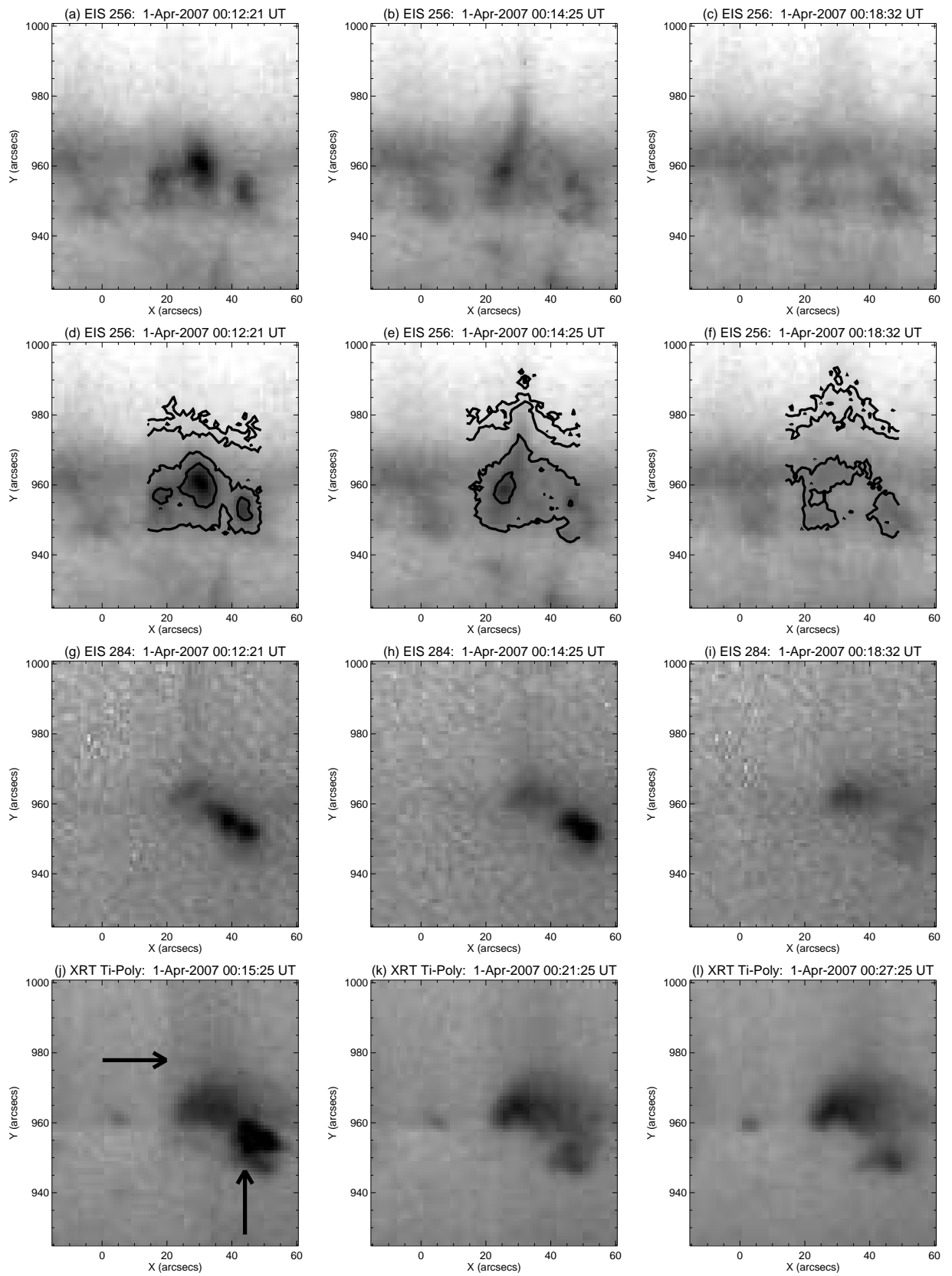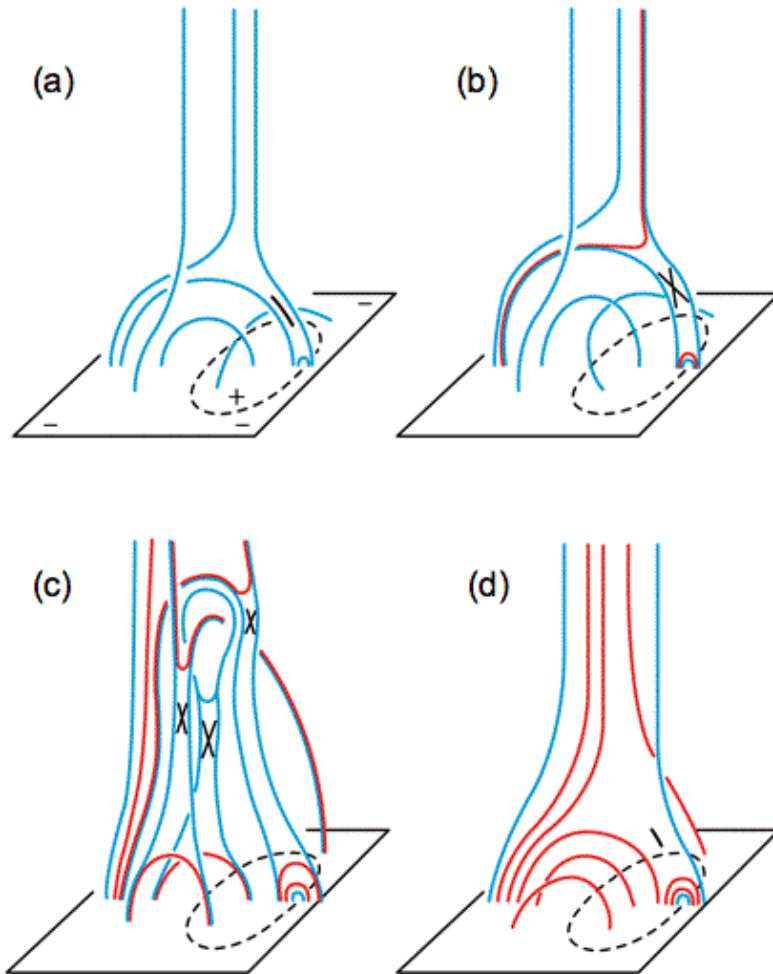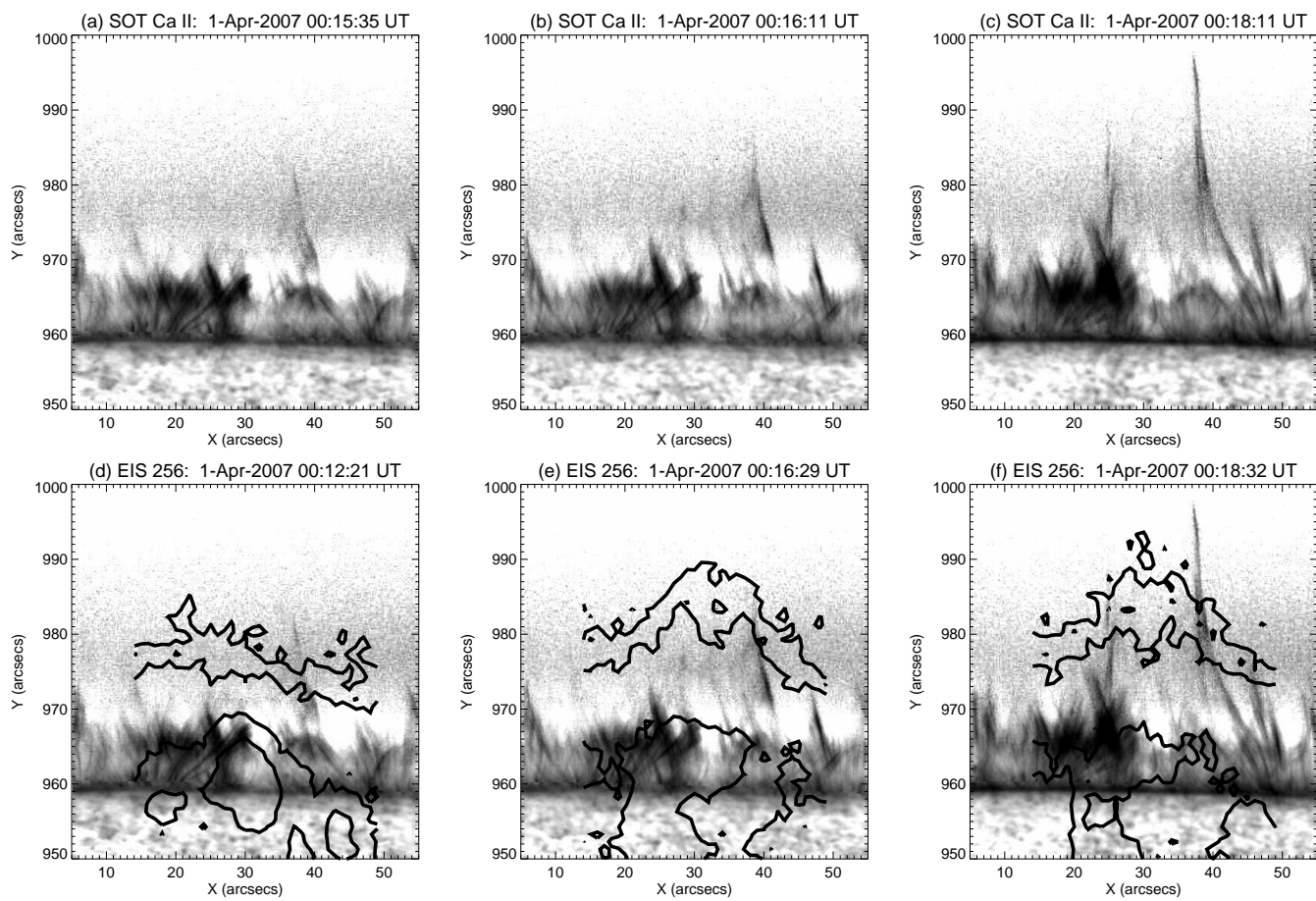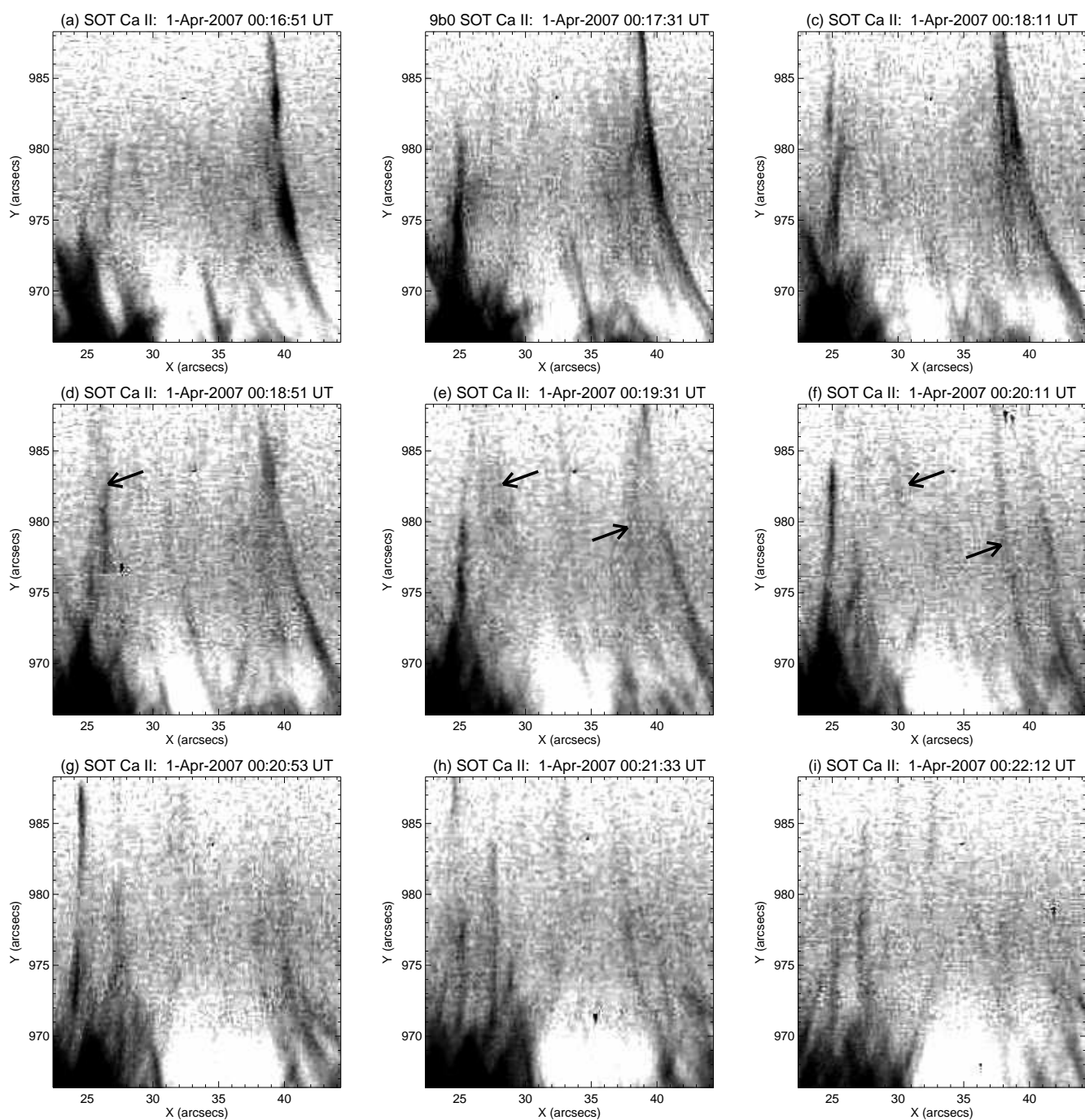
Figure 1

Figure 2

(a) SOT Ca II: 1-Apr-2007 00:15:35 UT

(b) SOT Ca II: 1-Apr-2007 00:16:11 UT

(c) SOT Ca II: 1-Apr-2007 00:18:11 UT

(d) EIS 256: 1-Apr-2007 00:12:21 UT

(e) EIS 256: 1-Apr-2007 00:16:29 UT

(f) EIS 256: 1-Apr-2007 00:18:32 UT

Figure 3

Figure 4